

Self-trapping of nanoparticles by bound states in the continuumEvgeny N. Bulgakov and Almas F. Sadreev *Kirensky Institute of Physics, Federal Research Center KSC SB RAS, 660036 Krasnoyarsk, Russia*

(Received 17 August 2022; revised 15 October 2022; accepted 18 October 2022; published 31 October 2022)

In the first tutorial part of the paper, we show that equilibrium positions of small dielectric particles inside the Fabry-Perot resonator (FPR) are sensitive to a frequency of incident electromagnetic wave and size of particle. That elucidates basic principles of resonant trapping of nanoparticles by excitation of high- Q resonances of FPR. In the second part, we consider a long dielectric cylinder with submicron radius (primary cylinder) integrated into a metallic waveguide which supports symmetry-protected bound states in the continuum (BICs). We consider the case of a slightly shifted cylinder relative to the axis of symmetry of a waveguide that controls the Q factor of quasi-BIC. Then, the extra nanoparticle perturbs quasi-BIC as dependent on the size of the nanoparticle and position relative to the primary cylinder. An interplay between the resonant width of quasi-BIC and a degree of frequency perturbation defines whether a dragging nanoparticle is terminated at a surface of the primary cylinder for an ultrasmall size of nanoparticles or at the definite distances from the cylinder for the larger size of nanoparticles. Thereby, we demonstrate a paradigm of resonant self-trapping and sorting of nanoparticles by use of quasi-BICs. We also show extremal sensitivity of self-trapping to the frequency of an electromagnetic (EM) wave propagating over waveguide.

DOI: [10.1103/PhysRevB.106.165430](https://doi.org/10.1103/PhysRevB.106.165430)**I. INTRODUCTION**

The experimental demonstration of optical separation using extended optical lattice or holographic methods in the presence of a laminar flow has shown in Refs. [1,2], which has been followed by theoretical analysis [3]. A generic method for sorting of micron particles based on the interference of two laser beams was considered and experimentally realized in Refs. [4,5]. However, sorting smaller nanoparticles whose sizes are substantially less than the optical wavelength needs different approaches. In the present paper, we consider the approach based on resonant enhancement of optical forces by excitation of bound states in the continuum (BICs) [6]. First, sharp features in the force spectrum, causing mutual attraction or repulsion between successive photonic crystal layers of dielectric spheres under illumination of a plane wave, has been established by Antonoyiannakis and Pendry [7]. It was revealed that the lower frequency bonding resonance forces push the two layers together, and the higher frequency antibonding resonance forces pull them apart. Later, these disclosures were reported for coupled photonic crystal slabs [8], two planar dielectric photonic metamaterials [9], a dimerized high-contrast grating with a compliant bilayer structure [10], and even in a single high-contrast dielectric resonator close to metal surface [11].

Mostly, the optical trapping is given by the Ashkin force which is proportional to gradient of electromagnetic power $\nabla|E|^2$ and, therefore, particles are trapped at the region of maximal intensity [12]. Optical trapping has found many applications in the physical and life sciences because it allows for precise control and positioning of micrometer-sized dielectric objects [13]. For example, optical trapping has

been applied to objects of biological interest, such as cells, bacteria, and viruses, to indirectly manipulate DNA and to measure the forces involved in RNA transcription [14]. There are fundamental challenges in extending optical trapping to nanoscale objects smaller than 100 nm. The gradient optical force becomes much weaker as the object gets smaller, scaling with the third power of its size. So far, the only approach to trap smaller objects has been to increase the trapping laser intensity. Consequently, trapping very small objects involves intensities that can exceed their damage threshold.

In this paper, we show first that BICs can be engaged for optical trapping of ultrasmall dielectric particles up to a few nm, applying a relatively small power electromagnetic wave of power around $1 \text{ mW}/\mu\text{m}$. Moreover, we demonstrate that nanoparticles dragging by air or liquid laminar flow in metallic waveguides are kept at definite positions relative to the primary dielectric cylinder integrated into the waveguide, and these positions are very sensitive to the size of dragging particles. As sketched in Fig. 1(a), the waveguide formed by two perfectly conducting metallic planes at a distance d holds a dielectric cylinder with refractive index $n = \sqrt{\epsilon}$ and radius R . The TM solutions of the Maxwell equations with electric field along the cylinder in such a system are equivalent to the solutions of periodic array of dielectric cylinders in air [15] that supports bound states in the radiation continuum (BICs) [16–32].

We consider the possibility of optical trapping of nanoparticles owing to extremely high sensitivity of quasi-BIC solution onto a presence of the particle near the primary cylinder. That mechanism is different from the so-called self-induced back-action optical trapping enhanced by the use of an optical resonance of the nanoparticle [33]. The property of

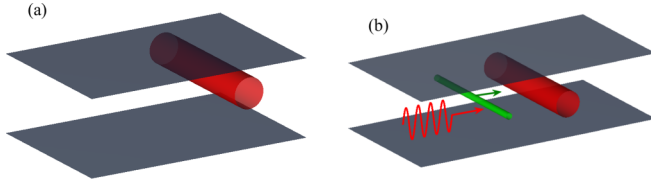


FIG. 1. (a) An infinitely long dielectric cylinder between two metallic planes. (b) The case under consideration: small (thin) cylinder moves parallel to reference cylinder.

giant enhancement of the response of the system supporting BICs is widely used in various applications of BICs, especially in sensing. However, that property is not enough for sorting of particles, for example, by sizes, because a magnitude of optical force is proportional to the area of particle. We consider the more sophisticated case when the system is almost tuned to the situation close to BIC. Then, a small dielectric particle approaching the system slightly perturbs the system and slightly shifts the resonant frequency of the system plus the nanoparticle. If the shifted frequency approaches close to the BIC frequency, the optical force enhanced by the Q factor of the system becomes extremely large. The perturbation of resonant frequency by small particles was considered by many scholars [34–36] and sensitive parameters of the small particles, such as size and shape, position, and refractive index of particles. Therefore, engagement of the BICs for sorting of particles promises to give us perspective in view of sorting the nanoparticles. In the present paper, we present the basic principles of sorting particles by use of high- Q modes of the Fabry-Perot resonator (FPR) and symmetry-protected (SP) BICs supported by single dielectric primary rod fixed in metallic waveguides as shown in Fig. 1.

II. RESONANT TRAPPING OF SMALL PARTICLES IN FABRY-PEROT RESONATOR

To illustrate principles of resonant trapping of small particles by high Q -resonant modes, we consider radiation pressure-driven FPR [37,38]. The FPR is formed by two high-contrast dielectric layers supporting resonances given by an number of the half wavelengths between layers [39]. Assume the distance between layers of the FPR slightly differs from the high- Q resonance. It is clear that a small particle modeled by a thin intermediate low-contrast layer inside the FPR perturbs the solution insignificantly. But the perturbation could be sufficient to tune the total system onto the high- Q resonance and, respectively, can cause significant changes of optical pressure as dependent on a position of the particle. The total system is sketched in Fig. 2. That reduces the problem to the one-dimensional case and enables analytic consideration of optical forces acting on the particle by use of the transfer matrix [40].

The solution in each spatial domain is given by the transfer matrices [38,40]

$$\begin{bmatrix} A \\ B \end{bmatrix} = \mathbf{M} \begin{bmatrix} 1 \\ R \end{bmatrix}, \quad \begin{bmatrix} T \\ 0 \end{bmatrix} = \mathbf{M} \begin{bmatrix} C e^{ik(L-x-\delta)} \\ D e^{-ik(L-x-\delta)} \end{bmatrix}, \quad (1)$$

$$\begin{bmatrix} C e^{ik(x-\delta)} \\ D e^{-ik(x-\delta)} \end{bmatrix} = \mathbf{m} \begin{bmatrix} A e^{ikx} \\ B e^{-ikx} \end{bmatrix}, \quad (2)$$

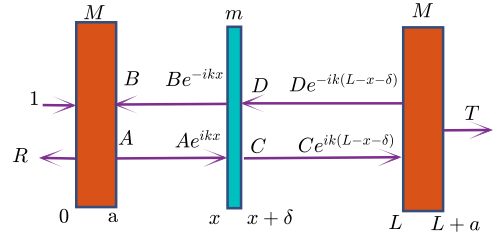


FIG. 2. Two dielectric slabs with refractive index n_0 and thickness a with thin dielectric slab with refractive index n and thickness δ .

where the transfer matrices are given [40] for slabs of FPR with thickness a and permittivity ϵ_0 :

$$\begin{aligned} M_{11} &= \cos(q_0 a) + \frac{i}{2} \left[\frac{q_0}{k} + \frac{k}{q_0} \right] \sin(q_0 a), \\ M_{12} &= \frac{i}{2} \left[\frac{q_0}{k} - \frac{k}{q_0} \right] \sin(q_0 a), \quad M_{22} = M_{11}^*, \quad M_{21} = M_{12}^*, \\ t &= \frac{1}{M_{22}}, \quad r = \frac{M_{12}}{M_{22}}. \end{aligned} \quad (3)$$

Here k and q are the wave vector components along the x axis:

$$k^2 = \omega^2 - \pi^2, \quad q_0^2 = \epsilon_0 k^2 + (\epsilon_0 - 1)\pi^2. \quad (4)$$

Respectively, for the transfer matrix of thin layer with thickness δ and permittivity ϵ , we have

$$\begin{aligned} m_{11} &= \cos(q\delta) + \frac{i}{2} \left[\frac{q}{k} + \frac{k}{q} \right] \sin(q\delta), \\ m_{12} &= \frac{i}{2} \left[\frac{q}{k} - \frac{k}{q} \right] \sin(q\delta), \quad m_{22} = m_{11}^*, \quad m_{21} = m_{12}^*, \end{aligned} \quad (5)$$

and

$$q^2 = \epsilon k^2 + (\epsilon - 1)\pi^2. \quad (6)$$

Following Refs. [37,38], we write for optical pressure (the force per unit area of thin layer)

$$P(x) = P_0 (|A(x)|^2 + |B(x)|^2 - |C(x)|^2 - |D(x)|^2), \quad (7)$$

where $P_0 = \frac{|E_0|^2}{8\pi} (\frac{k}{\pi})^2$ and E_0 is the amplitude of electromagnetic (EM) field. The results of simple numerics are presented in Fig. 3 which shows that the pressure completely correlates with the transmittance. For small perturbation of high- Q resonant mode $E_{z,n} = E_0 \sin(\pi n x / L)$, $n = 1, 2, 3, \dots$ inside the FPR, we can calculate perturbation shift of the resonant frequencies by use of the formula [34–36]

$$\begin{aligned} \Delta\omega_n &= -\frac{\omega_n(\epsilon - 1)}{2} \int_x^{x+\delta} E_{z,n}(x)^2 dx \\ &\approx -\frac{\pi n \delta (\epsilon - 1) E_0^2}{2L} \sin^2(\pi n x / L). \end{aligned} \quad (8)$$

One can see that the transmittance follows this formula for $\delta = 0.02$ as shown in Fig. 3(a), and the optical pressure follows the Ashkin gradient force

$$P = P_0 \frac{d|E_{z,n}|^2}{dx} = \frac{P_0}{2} \sin 2\pi n x / L,$$

as seen from Fig. 3(b).

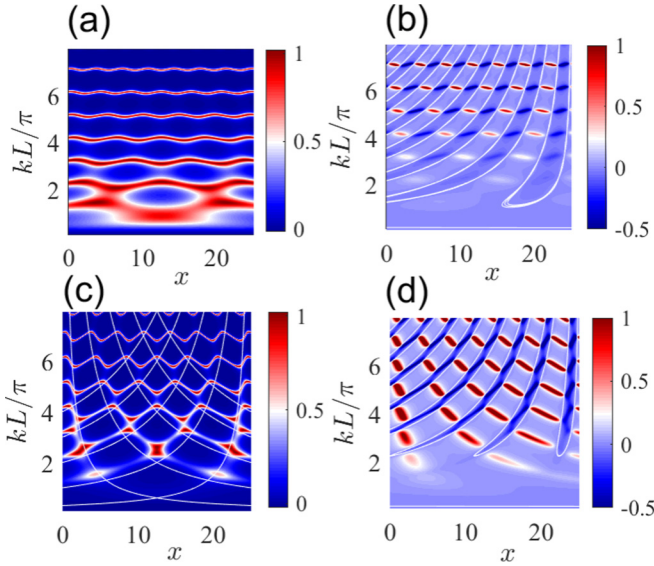


FIG. 3. Transmittance and optical pressure in arbitrary units rendered by plane wave at thin dielectric layer inside FPR. $a_0 = 1$, $\epsilon_0 = 10$, $\epsilon = 2$. White lines show equilibrium positions of thin layer. (a) and (b) $\delta = 0.02$, and (c) and (d) $\delta = 0.1$.

However, that is correct for a small perturbation exerting by small particle. With increasing thickness of the intermediate layer, the perturbed resonant mode cannot be described as the resonant mode of the empty FPR. It is easy to understand the origin of the resonant behavior of the transmittance shown in Fig. 3(c) for a thicker inner layer with $\delta = 0.1$ if we present the total system as two FPRs with two lengths x and $L - x$. Respectively, the left FPR has resonances at $k_n^L \approx \pi n_L/x$ while the right FPR has resonances at $k_n^R \approx \pi n_R/(L - x)$, where n_L and n_R are positive integers. As the resonances are crossing, we observe avoided crossing that Fig. 3(c) clearly demonstrates.

Optical force can reach significant values at the resonances with sufficiently high Q factors [38,41]. Because of propagating the plane wave from the left to the right, the pushing forces exceed the pulling forces. One can see from Eq. (9) the force is proportional to the thickness of layer that also correlates with Fig. 3. Figure 4 shows equilibrium positions of the thin particle inside the FPR as dependent on thickness. Therefore, one can select the particles of definite size by proper choice of the frequency of illumination or, equivalently, by proper choice of the length L of the FPR.

III. RESONANT TRAPPING OF NANOPARTICLES IN METALLIC WAVEGUIDE WITH DIELECTRIC CYLINDER

In this section, we explore the system sketched in Fig. 1(a) which supports abundance of different BICs, among which the SP are the most easy to achieve [15]. As analyzed in this paper, BICs in metallic waveguides with integrated dielectric rods are equivalent to BICs in the periodical array of rods. Thereby, we use the methods of solution of the Maxwell equations developed by Yasumoto and Jia [42] for multilayer two-dimensional photonic crystal structures.

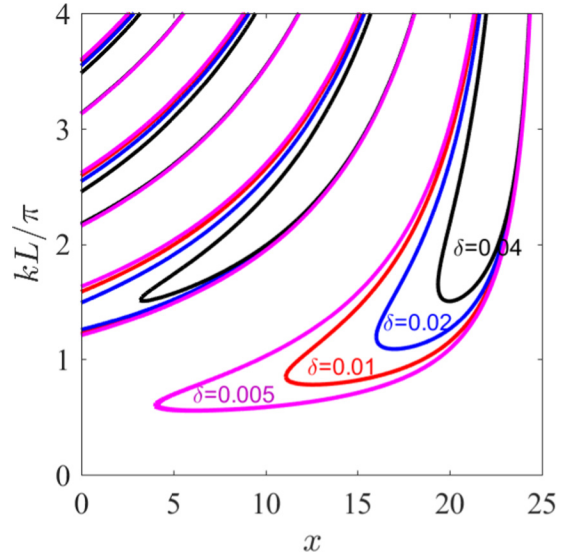


FIG. 4. Equilibrium positions of thin layers with different thicknesses δ at the parameters listed in Fig. 3.

In the first step, we solve the homogeneous Maxwell equations to establish the SP BICs as the resonant eigenmodes with real eigenfrequencies. It is clear that for the dielectric rod with the refractive index n_0 to trap the EM wave, its radius R has to be comparable with the characteristic wavelength inside the cylinder $\frac{2\pi}{n_0 k}$. Therefore, the threshold for SP BICs can be evaluated as $Rn_0 \approx C$, where the constant C of the order of magnitude of the unit depends on specific type of SP BIC [15]. In what follows, we take $R = 0.15$, $\epsilon_0 = 15$, where sizes and wave number are given in terms of the width of waveguide d . Numerically calculated behavior for thresholds of dipole (closed circles) and quadruple (open circles) types of SP BICs are presented in Fig. 5(a). Comparisons to this evaluated formula are shown by solid lines with $C = 0.3$ and $C = 0.6$, respectively. The only condition for the SP BICs to exist is the symmetrical position of the cylinder relative to the waveguide. Therefore, a shift of dielectric cylinder by distance Δ from the center line controls the Q factor of the quasi-BIC as shown in Fig. 5(b), where the Q factor is given by the ratio $\frac{\text{Re}(k)}{2\text{Im}(k)}$. The SP BICs can be labeled by orbital momentum $l = 1, 2, 3, \dots$ provided that the frequencies of the BICs are

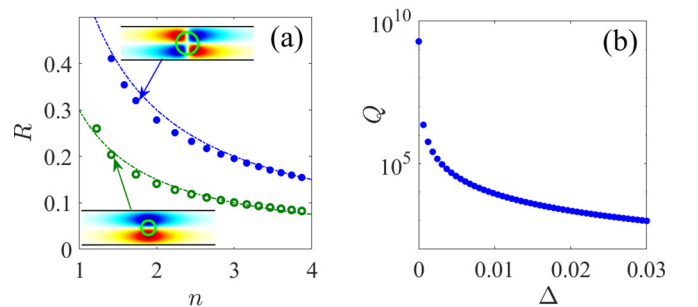


FIG. 5. (a) Curves of thresholds above which the SP BICs exist versus refractive index and radius of circular rod. (b) The Q factor of the quasi-SP BIC versus shift of cylindrical rod with $R = 0.15$, $\epsilon = 15$ relative to central line of waveguide.

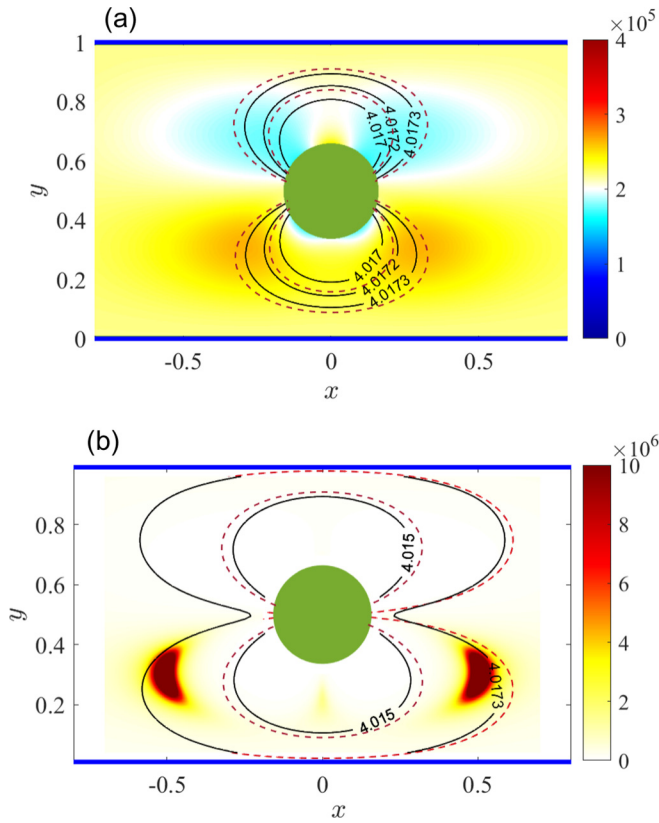


FIG. 6. The Q factor (color map) and contours of eigenfrequencies (solid lines) of the total system as dependent on position of nanoparticle in waveguide. Parameters of primary cylinder: $R = 0.15$, $\Delta = 0.002$, $\epsilon_0 = 15$ and nanoparticle : $\epsilon = 3$ and radii (a) $a = 0.01$ and (b) $a = 0.04$ in terms of waveguide width. Dashed line responses for the resonant frequency given by the perturbation theory.

below the second cutoff of the waveguide $2\pi c/d$, where c is the light velocity. In the present paper, we consider the SP BICs with $l = 1$ (dipole type) and $l = 2$ (quadruple type) whose profiles of electric field E_z are seen in Fig. 5(a).

Next, we assume that noninteracting (dilute concentration) nanoparticles are dragged by liquid or air flowing over a metallic waveguide as sketched in Fig. 1(b). To elaborate the basic principles of trapping and sorting of nanoparticles by sizes through an excitation of quasi-SP BICs, we model the nanoparticle as a thin dielectric cylinder parallel to the primary cylinder that reduces the dimension of the problem till two. We consider the dragging cylinder with permittivity ϵ has an extremely small radius $a \ll R$. One can expect that the presence of a nanoparticle in the waveguide perturbs the system and transforms the true SP BIC into quasi-BIC similar to the effect of structural imperfections [43–46]. However, there might be the opposite effect. Assume the primary cylinder in the waveguide is slightly shifted relative to central line of the waveguide by distance Δ that deflects the true SP BIC into quasi-BIC with a large but finite Q factor as shown in Fig. 5(b). Next, assume the nanoparticle is approached by the primary cylinder. If the perturbation by the nanoparticle is not sufficient to push the solution to the BIC solution, we observe gradual variation of the Q factor with the position of nanoparticle with the radius $a = 0.01$ as shown in Fig. 6(a).

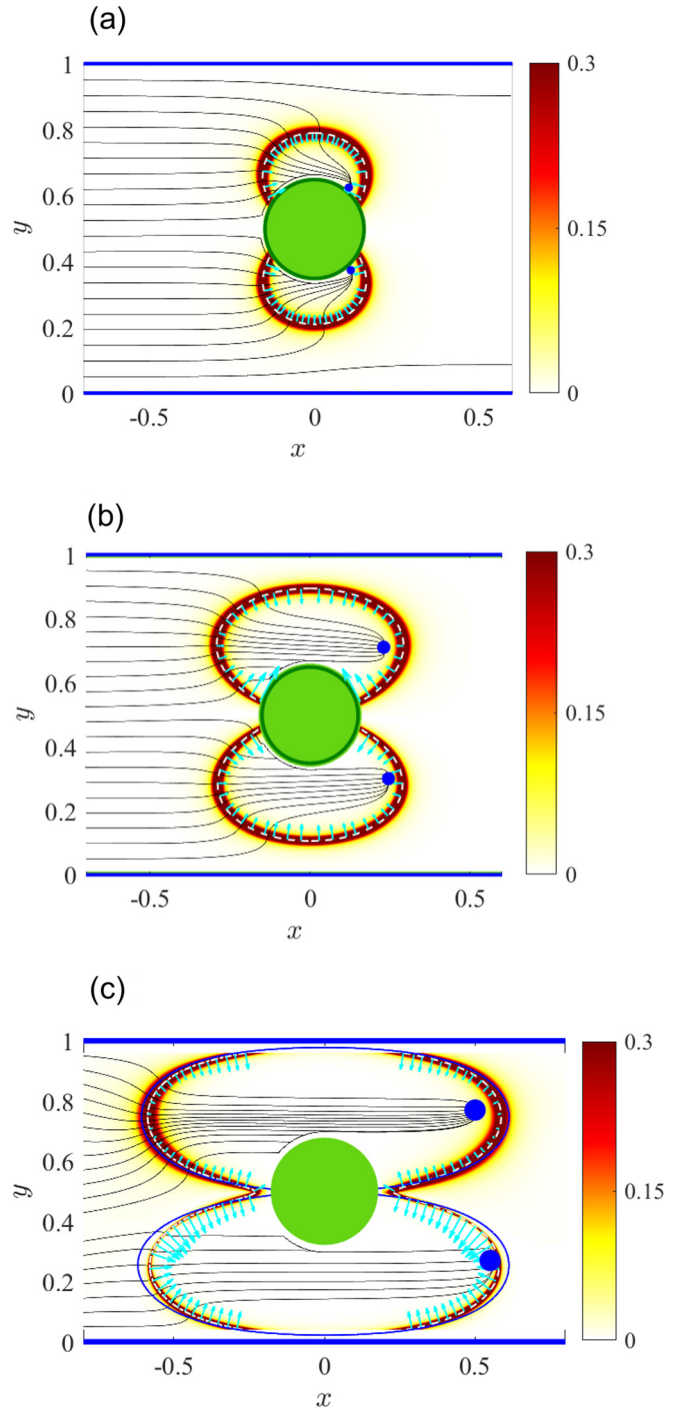


FIG. 7. Optical force $|\mathbf{F}|$ [$n\text{N}/\mu\text{m}$] (color map) and its directions (arrows) at the frequency $kd = 4.0173$ at different radii of nanoparticle: (a) $a = 0.005$, (b) $a = 0.01$, and (c) $a = 0.04$. Solid thin lines show trajectories of nanoparticles at different initial positions y and $x = -1$. Closed circles mark equilibrium positions of particles. The primary cylinder is shifted by $\Delta = 0.002$, $F_0 = 30$ pN/ μm , injected power equals 1 mW/ μm .

The real parts of the perturbed complex eigenfrequencies are shown by solid lines while the imaginary parts are shown by means of the Q factor. However, to increase the perturbation caused by the nanoparticle one sees in Figure 6(b), first, strong

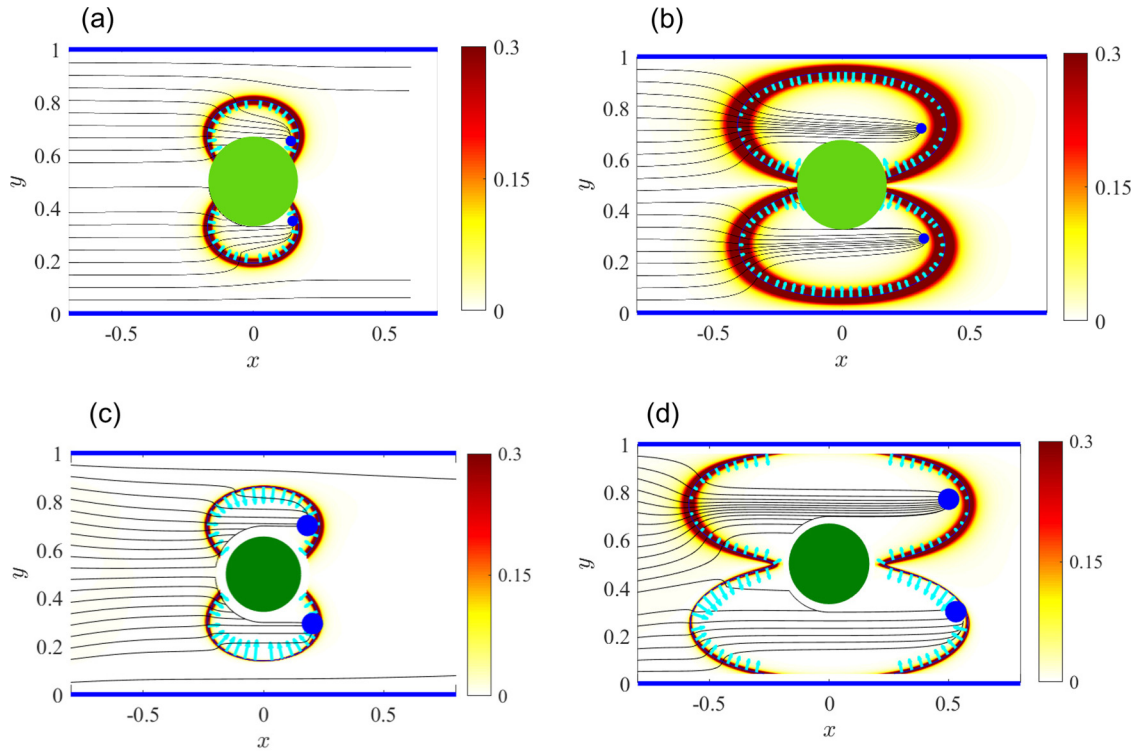


FIG. 8. Optical force $|\mathbf{F}|$ acting on ultrasmall particles at different frequencies of incident wave (a) $kd = 4.017$ and (b) $kd = 4.0174$ with radius $a = 0.01$ (upper panel); (c) $kd = 4.013$ and (d) $kd = 4.017$ with radius $a = 0.04$ (bottom panel). All other parameters are given in previous figures.

enhancement of the Q factor by two orders in magnitude and, second, quasi-BIC with an extremely high- Q factor is restored for selected positions of the nanoparticle. Also, we show in Fig. 6 that numerically calculated resonant frequencies of the total system (solid black lines) are close to the perturbation theory results (dashed lines) [34–36]:

$$\Delta \text{Re}(k) = -\frac{\text{Re}(k)(\epsilon - 1)}{2} \int d^2 \vec{x} |E_r(x)|^2. \quad (9)$$

Here integration is performed over the area of the small cylinder with the radius $a \ll R$ modeling the nanoparticle. Profiles of the scattering waves for a given amplitude of the incident wave are very close to the BIC solutions [23]. The only effect is related to strong resonant enhancement of the response proportional to $Q^{1/2}$. The current case is not an exception—the electromagnetic wave propagates over waveguide from the left and gives the scattering wave function close to the BIC solutions shown in Fig. 4(a) because of smallness of the nanoparticle. If we take $d = 1 \mu\text{m}$, these cases imply the sizes of the nanoparticle range from $a = 50 \text{ nm}$ to $a = 40 \text{ nm}$, which is considerably less than the radius of the primary cylinder.

In the second step, we calculate the optical force acting onto a small cylinder by excitation of quasi-BIC by external TM wave propagating along the metallic waveguide whose electric field is directed along cylinders. Results of the numerical calculation of optical force according to the theory of

electromagnetic force via the stress tensor [6],

$$F_i = \int T_{ij} dS_j, \\ T_{ij} = \frac{1}{4\pi} E_i E_j^* - \frac{1}{8\pi} \delta_{ij} |\mathbf{E}|^2 + \frac{1}{4\pi} H_i H_j^* - \frac{1}{8\pi} \delta_{ij} |\mathbf{H}|^2, \quad (10)$$

are shown in Figs. 7(a)–7(c) for three choices of the size of ananoparticle $a = 0.005$ (a), $a = 0.01$ (b), and $a = 0.04$ (c). Here the indices i, j numerate components in the cylindrical system of coordinates. For nanoparticles the optical force calculated by Eq. (10) is well approximated by the Ashkin formula [12], $\mathbf{F} = -\frac{\alpha}{2} \nabla |E_z|^2$, where α is the polarizability of the particle and E_z is the electric field directed along the z axis. The absolute value of force $\sqrt{F_x^2 + F_y^2}$ is proportional to the Q factor and therefore reaches extremely large values at those positions of the nanoparticle with the maximal Q factor shown in Fig. 6(b). For rather low power $1 \text{ mW}/\mu\text{m}$ of an electromagnetic wave propagating over the waveguide from the left to right, the force reaches giant magnitude $720 \text{ nN}/\mu\text{m}$. The directions of the force in Fig. 7 are shown by blue arrows.

However, in what follows we show that for optical self-trapping of nanoparticles, considerably lower resonant forces have importance. Assume that nanoparticles are dragged by the flow of air or liquid that is described by equation

$$\frac{d\mathbf{x}}{dt} = \mathbf{F} + \mathbf{e}_x F_0, \quad (11)$$

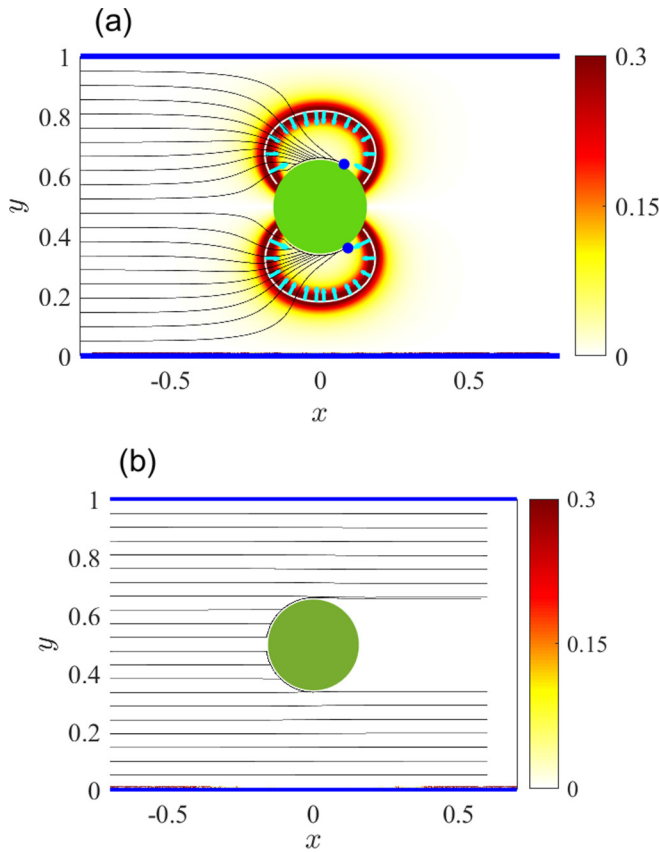


FIG. 9. The same as in Fig. 8 but for smaller nanoparticle with $a = 0.0025$. (a) $kd = 4.0174$ and (b) $kd = 4.017$.

where the last term describes the dragging force directed along the waveguide and the friction coefficient at a velocity of nanoparticle is absorbed by time. Solid thin lines in Fig. 7 show trajectories of nanoparticles which evolve since initial position $x = -1$. These trajectories unambiguously demonstrate that owing to excitation of high- Q resonant modes close to the SP BIC by the propagating wave, the primary cylinder in the waveguide effectively manipulates viscous motion of nanoparticles.

One can see from Fig. 7 that curves of definite fixed resonant frequencies form two arcs above and below the primary cylinder, which are extending with growth of the nanoparticle's size for the dipole-type quasi-SP BIC. Respectively, an electromagnetic wave resonant to these frequencies gives rise to resonant optical forces which follow these arcs. These arc forces exceed by two orders in magnitude nonresonant forces (white background) as seen from Fig. 7, and have a key importance in a resonant self-trapping of nanoparticles inside arcs. As soon as nanoparticle deviates from these arcs the force drastically falls down and can be balanced by weak dragging force right near the arcs. Moreover, the x component of vectorial forces at the right arcs is opposite to forces at the left arcs as one sees from Fig. 7 and the following figures. Thereby, the drag force directed to the right can be compensated only around the right arcs to result in full termination of the nanoparticle at places marked by a closed circle. In accordance with Eq. (9), the size of the resonant arc increases with the volume of the nanoparticle. That mechanism elaborates a

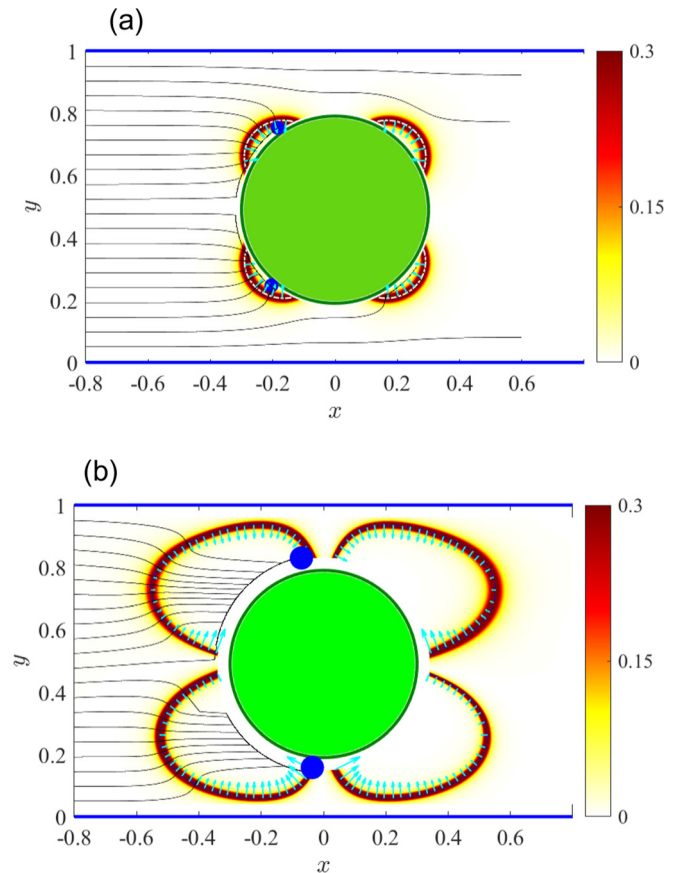


FIG. 10. Evolution of nanoparticles with initial position $x = -1$ under excitation of the quadruple quasi-SP BIC solution by electromagnetic wave with power $1 \text{ mW}/\mu\text{m}$ and frequency $kd = 3.28$ for two radii of nanoparticles: (a) $a = 0.01$ and (b) $a = 0.04$. The primary cylinder with the radius $R = 0.3$ and $\epsilon = 15$ is shifted by $\Delta = 0.01$.

paradigm of the resonant sorting of nanoparticles by its sizes as shown in Figs. 7(a)–7(c).

The above considered paradigm of resonant optical self-trapping forces brings a new parameter to manipulate by sorting the particles, by a frequency of electromagnetic power. As Fig. 6 shows, a slight variation of resonant frequency drastically changes the radius of the arcs. Respectively, one expects that for nanoparticles of selected size, a slight change of the frequency of propagating electromagnetic wave will drastically change the final position of the nanoparticles, as Fig. 8 demonstrates for nanoparticles of two sizes: $a = 0.01$ and $a = 0.04$. Moreover, one can see from this figure that the more the size of the particle, the more change in frequency of the propagating EM wave is necessary. Figure 9 shows a striking effect of blockage of nanoparticles with the radius $a = 0.0025$ that constitutes only a few nanometers in optical range by the slightest change of frequency of electromagnetic wave for 0.04%.

The case of quadruple quasi-SP BIC obviously will form four arcs of resonant frequencies along which the giant resonant optical force are arranged. Accordingly, Fig. 10 shows the corresponding distribution of optical forces and evolution of the nanoparticle under the effect of total force on the

right-hand side of Eq. (11). Differently from the case of excitation of dipole quasi-BIC, in the present case quadruple quasi-BIC nanoparticles are terminated at the surface of the primary cylinder independently of the size of the nanoparticles.

IV. CONCLUSIONS

The aim of the present paper was a demonstration of basic principles of resonant self-trapping of nanoparticles with sizes much less than the wavelength by use of high- Q resonances in the FPR or in a metallic waveguide with an integrated high-contrast dielectric cylinder. Owing to that, nanoparticles can considerably effect the solution as dependent on a vicinity of the solution to the BIC. As for a system which can support BICs, we consider a dielectric long high-contrast cylinder integrated into a metallic waveguide [15]. That system also has an advantage by a possibility to drag nanoparticles by air of liquid flowing over a waveguide. For approaching nanoparticles to the primary cylinder, there can be two basic scenarios for trapping nanoparticles as dependent on comparison between the frequency perturbation given by Eq. (9) and the resonant width of quasi-BIC. In the first scenario, the nanoparticle perturbs the solution so weakly that the optical force can be described by the optical force without involvement of the nanoparticle. Our calculations show that force traps the nanoparticle on a surface of the primary cylinder. In the

second scenario, the perturbation can be sufficient to excite high- Q resonant modes or quasi-BIC. However, that happens for only definite positions of nanoparticles relative to the primary cylinder. Because of the high sensitivity of equilibrium positions of nanoparticles to their sizes, we demonstrate means of resonant self-trapping and sorting of nanoparticles. Moreover, we demonstrate extremely high sensitivity of this effect on the frequency of electromagnetic wave propagating over waveguide. Therefore, both models demonstrate the key result of a manipulation position of small particles as dependent on their sizes and frequency of illumination, i.e., sorting.

It is remarkable that the similar TM SP BICs exist in metallic waveguides of cross-section $L_x \times L_y$ with symmetrically integrated dielectric cylinder of the length L_y or L_x with an electric field directed along the cylinder [15]. That opens a way of sorting submicron particles of finite sizes. If we assume the particles have a spherical shape with radius a , the perturbed resonant frequencies will be diminished by a factor a/L_x . Moreover, the Q factor of quasi-BIC is restricted by the surface impedance of a metallic waveguide and material losses of the primary cylinder. These adverse effects are to be accounted for in future studies.

ACKNOWLEDGMENT

The work was supported by Russian Science Foundation Grant No. 22-12-00070.

-
- [1] M. P. MacDonald, G. C. Spalding, and K. Dholakia, Microfluidic sorting in an optical lattice, *Nature (London)* **426**, 421 (2003).
- [2] K. Ladavac, K. Kasza, and D. G. Grier, Sorting mesoscopic objects with periodic potential landscapes: Optical fractionation, *Phys. Rev. E* **70**, 010901(R) (2004).
- [3] A. M. Lacasta, J. M. Sancho, A. H. Romero, and K. Lindenberg, Sorting on Periodic Surfaces, *Phys. Rev. Lett.* **94**, 160601 (2005).
- [4] T. Čižmár, M. Šiler, M. Šerý, P. Zemánek, V. Garcés-Chávez, and K. Dholakia, Optical sorting and detection of submicrometer objects in a motional standing wave, *Phys. Rev. B* **74**, 035105 (2006).
- [5] O. Brzobohatý, V. Karásek, M. Šiler, L. Chvátal, T. Čižmár, and P. Zemánek, Experimental demonstration of optical transport, sorting and self-arrangement using a ‘tractor beam,’ *Nat. Photon.* **7**, 123 (2013).
- [6] M. I. Antonoyiannakis and J. B. Pendry, Electromagnetic forces in photonic crystals, *Phys. Rev. B* **60**, 2363 (1999).
- [7] M. I. Antonoyiannakis and J. B. Pendry, Mie resonances and bonding in photonic crystals, *Europhys. Lett.* **40**, 613 (1997).
- [8] V. Liu, M. Povinelli, and S. Fan, Resonance-enhanced optical forces between coupled photonic crystal slabs, *Opt. Express* **17**, 21897 (2009).
- [9] J. Zhang, K. F. MacDonald, and N. I. Zheludev, Giant optical forces in planar dielectric photonic metamaterials, *Opt. Lett.* **39**, 4883 (2014).
- [10] C. B. R. Hurtado, J. Dickmann, F. F. Bruns, T. Siefke, and S. Kroker, Bound states in the continuum for optomechanical light control with dielectric metasurfaces, *Opt. Express* **28**, 20106 (2020).
- [11] E. Bulgakov, K. Pichugin, and A. Sadreev, Resonant binding of dielectric particles to a metal surface without plasmonics, *Phys. Rev. A* **103**, L051501 (2021).
- [12] A. Ashkin, J. M. Dziedzic, J. E. Bjorkholm, and S. Chu, Observation of a single-beam gradient force optical trap for dielectric particles, *Opt. Lett.* **11**, 288 (1986).
- [13] K. Dholakia, P. Reece, and M. Gu, Optical micromanipulation, *Chem. Soc. Rev.* **37**, 42 (2008).
- [14] A. Ashkin and J. M. Dziedzic, Optical trapping and manipulation of viruses and bacteria, *Science* **235**, 1517 (1987).
- [15] E. Bulgakov, A. Pilipchuk, and A. Sadreev, Desktop laboratory of bound states in the continuum in metallic waveguide with dielectric cavities, *Phys. Rev. B* **106**, 075304 (2022).
- [16] P. Vincent and M. Nevière, Corrugated dielectric waveguides: A numerical study of the second-order stop bands, *Appl. Phys.* **20**, 345 (1979).
- [17] A.-S. Bonnet-Bendhia and F. Starling, Guided waves by electromagnetic gratings and non-uniqueness examples for the diffraction problem, *Math. Methods Appl. Sci.* **17**, 305 (1994).
- [18] V. Astratov, J. Culshaw, R. Stevenson, D. Whittaker, M. Skolnick, T. Krauss, and R. de la Rue, Resonant coupling of near-infrared radiation to photonic band structure waveguides, *J. Lightw. Technol.* **17**, 2050 (1999).
- [19] S. G. Tikhodeev, A. L. Yablonskii, E. A. Muljarov, N. A. Gippius, and T. Ishihara, Quasiguided modes and optical properties of photonic crystal slabs, *Phys. Rev. B* **66**, 045102 (2002).
- [20] S. P. Shipman and S. Venakides, Resonant transmission near nonrobust periodic slab modes, *Phys. Rev. E* **71**, 026611 (2005).
- [21] D. C. Marinica, A. G. Borisov, and S. V. Shabanov, Bound States in the Continuum in Photonics, *Phys. Rev. Lett.* **100**, 183902 (2008).

- [22] C. W. Hsu, B. Zhen, J. Lee, S. G. Johnson, J. D. Joannopoulos, and M. Soljačić, Observation of trapped light within the radiation continuum, *Nature (London)* **499**, 188 (2013).
- [23] E. N. Bulgakov and A. F. Sadreev, Bloch bound states in the radiation continuum in a periodic array of dielectric rods, *Phys. Rev. A* **90**, 053801 (2014).
- [24] Y. Yang, C. Peng, Y. Liang, Z. Li, and S. Noda, Analytical Perspective for Bound States in the Continuum in Photonic Crystal Slabs, *Phys. Rev. Lett.* **113**, 037401 (2014).
- [25] D. A. Bykov and L. L. Doskolovich, $\omega - kx$ Fano line shape in photonic crystal slabs, *Phys. Rev. A* **92**, 013845 (2015).
- [26] Z. Hu and Y. Y. Lu, Standing waves on two-dimensional periodic dielectric waveguides, *J. Opt.*, **17**, 065601 (2015).
- [27] C. W. Hsu, B. Zhen, S.-L. Chua, S. G. Johnson, J. D. Joannopoulos, and M. Soljačić, Bloch surface eigenstates within the radiation continuum, *Light Sci. Appl.* **2**, e84 (2013).
- [28] X. Gao, C. W. Hsu, B. Zhen, X. Lin, J. D. Joannopoulos, M. Soljačić, and H. Chen, Formation mechanism of guided resonances and bound states in the continuum in photonic crystal slabs, *Sci. Rep.* **6**, 31908 (2016).
- [29] Z. F. Sadrieva, I. S. Sinev, K. L. Koshelev, A. Samusev, I. V. Iorsh, O. Takayama, R. Malureanu, A. A. Bogdanov, and A. V. Lavrinenko, Transition from optical bound states in the continuum to leaky resonances: Role of substrate and roughness, *ACS Photon.* **4**, 723 (2017).
- [30] S.-G. Lee and R. Magnusson, Band flips and bound-state transitions in leaky-mode photonic lattices, *Phys. Rev. B* **99**, 045304 (2019).
- [31] S. Joseph, S. Sarkar, S. Khan, and J. Joseph, Exploring the optical bound state in the continuum in a dielectric grating coupled plasmonic hybrid system, *Adv. Opt. Mater.* **9**, 2001895 (2021).
- [32] F. Wu, C. Fan, K. Zhu, J. Wu, X. Qi, Y. Sun, S. Xiao, H. Jiang, and H. Chen, Tailoring electromagnetic responses in a coupled-grating system with combined modulation of near-field and far-field couplings, *Phys. Rev. B* **105**, 245417 (2022).
- [33] M. Juan, R. Gordon, Y. Pang, F. Eftekhari, and R. Quidant, Self-induced back-action optical trapping of dielectric nanoparticles, *Nat. Phys.* **5**, 915 (2009).
- [34] H. M. Lai, P. T. Leung, K. Young, P. W. Barber, and S. C. Hill, Time-independent perturbation for leaking electromagnetic modes in open systems with application to resonances in microdroplets, *Phys. Rev. A* **41**, 5187 (1990).
- [35] E. A. Muljarov, W. Langbein, and R. Zimmermann, Brillouin-Wigner perturbation theory in open electromagnetic systems, *Europhys. Lett.* **92**, 50010 (2010).
- [36] P. T. Kristensen, K. Herrmann, F. Intravaia, and K. Busch, Modeling electromagnetic resonators using quasinormal modes, *Adv. Opt. Photon.* **12**, 612 (2020).
- [37] J. K. Asbóth, H. Ritsch, and P. Domokos, Optomechanical coupling in a one-dimensional optical lattice, *Phys. Rev. A* **77**, 063424 (2008).
- [38] A. F. Sadreev and E. Y. Sherman, Temporal oscillations of light transmission through dielectric microparticles subjected to optically induced motion, *Phys. Rev. A* **94**, 033820 (2016).
- [39] M. Born, E. Wolf, A. B. Bhatia, P. C. Clemmow, D. Gabor, A. R. Stokes, A. M. Taylor, P. A. Wayman, and W. L. Wilcock, *Principles of Optics* (Cambridge University Press, Oxford, 1999).
- [40] P. Markoš and C. Soukoulis, *Wave Propagation: From Electrons to Photonic Crystals and Left-Handed Materials* Princeton Univ (Princeton University Press, Princeton, 2008).
- [41] M. L. Povinelli, S. G. Johnson, M. Loncar, M. Ibanescu, E. J. Smythe, F. Capasso, and J. D. Joannopoulos, High-Q enhancement of attractive and repulsive optical forces between coupled whispering-gallery-mode resonators, *Opt. Express* **13**, 8286 (2005).
- [42] K. Yasumoto and H. Jia, Modeling of photonic crystals by multilayered periodic arrays of circular cylinders, in *Electromagnetic Theory and Applications for Photonic Crystals*, edited by K. Yasumoto (MIT Press, Cambridge, MA, 2006), pp. 527–579.
- [43] L. Yuan and Y. Y. Lu, Bound states in the continuum on periodic structures: Perturbation theory and robustness, *Opt. Lett.* **42**, 4490 (2017).
- [44] L. Ni, J. Jin, C. Peng, and Z. Li, Analytical and statistical investigation on structural fluctuations induced radiation in photonic crystal slabs, *Opt. Express* **25**, 5580 (2017).
- [45] L. Yuan and Y. Y. Lu, Perturbation theories for symmetry-protected bound states in the continuum on two-dimensional periodic structures, *Phys. Rev. A* **101**, 043827 (2020).
- [46] E. Maslova, M. Rybin, A. Bogdanov, and Z. Sadrieva, Bound states in the continuum in periodic structures with structural disorder, *Nanophotonics* **10**, 4313 (2021).